Journal of Modern Optics
Vol. 53, Nos. 16–17, 10–20 November 2006, 2583–2591

Taylor & Francis
Taylor & Francis Group

Slow light in paraffin-coated Rb vapour cells

M. KLEIN*†‡, I. NOVIKOVA†, D. F. PHILLIPS† and R. L. WALSWORTH†‡

†Harvard-Smithsonian Center for Astrophysics, Cambridge, MA, 02138, USA
‡Department of Physics, Harvard University, Cambridge, MA, 02138, USA

(*Received 21 August 2006*)

Preliminary results from an experimental study of slow light in anti-relaxation-coated Rb vapour cells are presented, and the construction and testing of such cells are described. The slow ground state decoherence rate allowed by coated cell walls leads to a dual-structured electromagnetically induced transparency (EIT) spectrum with a very narrow (< 100 Hz) transparency peak on top of a broad pedestal. Such dual-structured EIT permits optical probe pulses to propagate with greatly reduced group velocity on two time scales. Ongoing efforts to optimize the pulse delay in such coated cell systems are discussed.

The manipulation of spin states in atomic ensembles lies at the heart of many quantum-optical effects [1, 2]. Such processes require high-quality state preparation and minimal decoherence of the spin state of the atomic ensemble. In warm atomic vapour cells, spin state lifetimes are often limited by wall collisions, which thermalize internal atomic states and destroy spin coherence. Coating the walls of the cell with a paraffin derivative allows atoms to undergo many wall-collisions without losing their spin coherence and prolongs spin lifetimes up to 1 second [3–5]. Paraffin-coated alkali-vapour cells have been successfully used to demonstrate spin squeezing [6], entanglement of atomic ensembles [7] and quantum memory for continuous quantum variables [8, 9], and are also used for high-precision atomic clocks and magnetometers [10–12].

In this paper we study electromagnetically induced transparency (EIT) [1, 13, 14] and slow light [15, 16] in paraffin-coated Rb cells, e.g., as a step towards the application of such vapour cells for a quantum memory [2, 17] in a quantum repeater [18] as well as for long delay times for classical pulses. In our present study, we characterize a dual-structured EIT spectrum which includes a very narrow central feature that allows ultra-slow group velocities for the propagation of weak classical pulses through the EIT medium [19].

*Corresponding author. Email: mklein@fas.harvard.edu

Journal of Modern Optics
ISSN 0950–0340 print/ISSN 1362–3044 online
http://www.tandf.co.uk/journals
DOI: 10.1080/09500340600952135

1. Cell coating procedure

Vapour cell coatings have been investigated for over 40 years utilising various techniques and derivatives of paraffin as a coating material [3, 20, 21]. Presently, we employ a technique similar to Alley and co-workers [22] for our cylindrical cell geometry. (In previous work [23], we used techniques similar to those described by Bouchiat [3] which was more appropriate to spherical vapour cells.) Following Robinson [4], we coat with tetracontane ($C_{40}H_{82}$), a readily available component of paraffin.

After thoroughly cleaning the vapour cell manifold and attaching it to the vacuum system (see figure 1(*a*)), we bake the manifold under vacuum at $\gtrsim$200°C. This further cleans the Pyrex glassware and reduces the base pressure of the system. The manifold is then cooled to room temperature and filled with N_2 gas to a pressure slightly above 1 atmosphere. A valve on the manifold is then removed allowing a glass rod, onto which a few flakes of tetracontane have been melted, into the cell. The valve is then reseated and the manifold evacuated.

To apply tetracontane to the cell walls, we enclose the cell in an oven composed of a thin aluminum box with attached resistive heater plates. The neck of the cell manifold is wrapped in resistive heater tape to provide additional heating of this region. The valve is then closed, isolating the cell from the rest of the vacuum system so that tetracontane does not escape the coating region during the coating process. The cell and neck are then heated to ~200°C to melt and vaporize the tetracontane with the neck region $\gtrsim$10°C warmer than the cell to keep tetracontane from accumulating in the neck. Finally, the cell is cooled to room temperature and the valve opened to the vacuum system so that any gas created during the coating process is pumped away. Visible tetracontane on the cell walls indicates cold spots during the coating process and thus the lack of a uniform coating layer over the surface. In this case, the process is repeated to improve the coating uniformity.

After the coating is successfully applied, natural abundance metallic Rb is distilled from its ampoule to the tip using a blown air heat gun. Bulk Rb is kept out of the main volume of the cell, as it can interact with the coating and damage it.

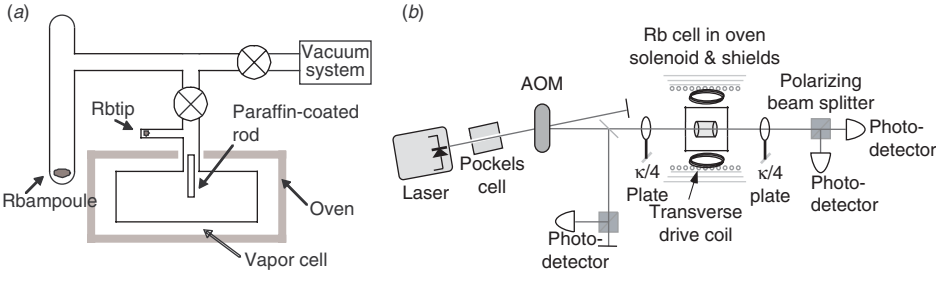

Figure 1. (*a*) Schematic of the Pyrex manifold and vacuum system used to apply paraffin coating to the inside of the cell. (*b*) Schematic of the apparatus for double resonance, EIT, and slow light experiments. *See text*.

Lastly, the coating rod is moved out of the cell and the cell is "pulled-off" from the manifold by melting the glass just above the Rb tip while also keeping the Rb tip cool. Once the vapour cell has been completed, the temperature of the Rb tip should be kept below that of the cell body so that bulk rubidium remains in the tip rather than in the body. Additionally, the cell body should be kept below 81°C, the melting point of tetracontane.

2. Apparatus

The experimental apparatus shown in figure 1(*b*) is used for testing the quality of the cell coating and for EIT and slow light measurements. An external cavity diode laser [24] tuned near the Rb D_1 line ($\lambda \approx 795$ nm) produces linearly polarized light which acts as a strong control field (Ω_C in figure 2). If needed, a weak probe field (Ω_P) is produced by rotating the optical polarization using a Pockels cell with a maximum probe to control field intensity ratio of 10:1. The total intensity is regulated using an acousto-optic modulator (AOM). After the AOM, a small fraction of the probe light is sent to a photo-detector (PD) as a reference for slow light delay measurements. Quarter-wave plates before and after the Rb cell convert the control and probe field polarizations from linear to circular and back. The maximum total laser power at the cell is 3 mW, weakly focused into a 2 mm diameter beam, except where noted below. The control and probe components are then measured using a polarizing beam splitter and two PDs.

The cylindrical tetracontane-coated Rb cell of length 5 cm and diameter 2.5 cm is housed inside four layers of magnetic shielding (to screen stray laboratory magnetic fields). The cell is heated conductively by blowing hot air through the plastic housing containing the vapour cell. A solenoid and sets of coils mounted around the cell allow us to apply a homogeneous magnetic field and a transverse rf field (Ω_{rf} in figure 2(*a*)) when needed.

3. Coated cell testing

We evaluate the coating quality by employing two complementary techniques to measure the atomic spin decoherence rate. In optical pumping double resonance [25], we illuminate the cell with circularly polarized light, optically pumping the atomic population to the state with maximum angular momentum $m_F = F$, so that the atomic vapour becomes transparent to the applied optical field. In the presence of a static longitudinal magnetic field which splits the Zeeman ground state sublevels, we apply a transverse rf magnetic field. If the rf field is resonant with the splitting of the ground state Zeeman sublevels, it mixes the population into other levels and thus increases the optical absorption. Sweeping the rf frequency through the Zeeman resonance produces a dip in the transmission spectrum allowing a determination of both the Zeeman frequency and its decoherence rate. For the example result shown in figure 2(*a*), we detected the change in transmission of a circularly polarized laser field tuned to a transition between the $F = 3$ ground state and unresolved excited

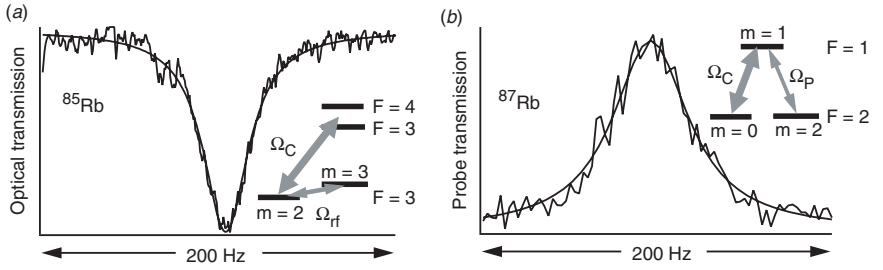

Figure 2. Ground-state Zeeman coherence measurements using (*a*) optical pumping double resonance (FWHM ≈ 22 Hz) with ≈ 0.8 mm beam diameter, and (*b*) EIT resonance (FWHM ≈ 50 Hz) with ≈ 2 mm beam diameter. Smooth curves are Lorentzian fits to the data. Laser intensity was 0.1 mW/cm^2 to avoid power broadening. *Insets*: interaction schemes for each measurement. Note that for the double resonance measurement we used ^{85}Rb, which has a larger natural abundance (72%) than ^{87}Rb, providing higher Rb density at the same cell temperature.

states of ^{85}Rb in a static, longitudinal magnetic field of ≈ 38 mG while sweeping the rf field frequency. The observed transmission dip in figure 2(*a*) had a full width of 22 Hz, corresponding to a Zeeman coherence lifetime ≈ 15 ms.

Alternatively, we measure the EIT linewidth by applying continuous control and probe optical fields with equal frequency and opposite circular polarizations, which optically pump the atoms into a coherent superposition of the ground-state Zeeman sublevels (i.e. a "dark state") [1]. Ideally, atoms in this state are completely decoupled from both optical fields and do not absorb any light. An applied magnetic field lifts the degeneracy of Zeeman sublevels and destroys the dark state, leading to greater optical absorption. For the example results shown in figure 2(*b*) (same Rb cell as in figure 2(*a*)), the control and probe fields were resonant with the $F = 2 \rightarrow F' = 1$ transition of ^{87}Rb, forming a Λ-system on the $m_F = 0$ and $m_F = +2$ ground-state Zeeman sublevels. The two-photon detuning was varied by slowly sweeping the longitudinal magnetic field near zero. The observed EIT resonance in figure 2(*b*) had a full width ≈ 50 Hz (coherence lifetime ≈ 6.6 ms).

In both double-resonance (DR) and EIT measurements, the width of the narrow resonance is limited by the decoherence rate of the Zeeman sublevels. To set a limit on the contribution of wall collisions, we work at low laser and rf field power to avoid power broadening. We also avoid broadening from Rb–Rb spin-exchange collisions by keeping the cell at a low temperature (36°C, corresponding to a Rb number density of 3×10^{10} cm^{-3}). We believe that uncompensated magnetic field gradients are the leading remaining decoherence source in both DR and EIT linewidth measurements, which is consistent with the approximate factor of two difference in the measured DR and EIT linewidths: for a fixed field gradient, the $\Delta m = 2$ EIT transition should have twice the frequency width of the $\Delta m = 1$ double resonance measurement. These results imply that the contribution of wall collisions to the Rb Zeeman decoherence rate is $\ll 10$ Hz.

4. Dual-structured EIT and slow light measurements

Figure 3 shows an example of the measured dual-structured EIT lineshape in a paraffin-coated Rb vapour cell. The EIT lineshape consists of two distinct features: a broad pedestal due to atoms interacting with the laser beam only once, and a narrow central peak due to atoms returning to the beam after multiple bounces from the walls (and thus having a much longer coherence lifetime). A comprehensive study of EIT lineshapes and slow light in coated cells will be presented in future publications.

We explored slow light pulse propagation over a wide range of experimental parameters (field intensities between 1 and 60 mW/cm^2, cell temperatures from 50 to 75°C, and pulse widths from 1 μs to 20 ms) (see figure 4). We found two distinct regimes of maximum fractional pulse delay, corresponding to the two frequency scales observed in the dual-structured EIT lineshapes. At high laser intensity, many atoms are pumped into the dark state on a time scale comparable to the transit time of an atom through the laser beam (as in an uncoated cell). This leads to an observed maximum fractional delay for pulse lengths near 10 μs (triangles in figure 4(*a*)), corresponding to the broad EIT pedestal in figure 3. At lower laser powers (squares in figure 4(*a*)), the maximal fractional delay is observed for much longer pulses with lengths of several milliseconds. These pulses match the narrow central feature of the EIT resonance of figure 3.

Naively, we expect broadening of output pulses (i.e. narrowing of the frequency spectrum) when the pulse bandwidth is larger than the EIT spectral window [26]. However, in these measurements, we typically observe negative fractional pulse reshaping (defined as the difference of the input and output pulse widths, normalized to the input pulse width) as shown in figure 4(*d*). We are currently studying this counterintuitive phenomenon in greater detail.

By adding a repumping beam on the lower energy hyperfine level, we can increase the number of atoms interacting with the laser fields without increasing the atomic density. The repumper (Ω_R in figure 5(*a*)) depopulates the $F = 1$ hyperfine ground state

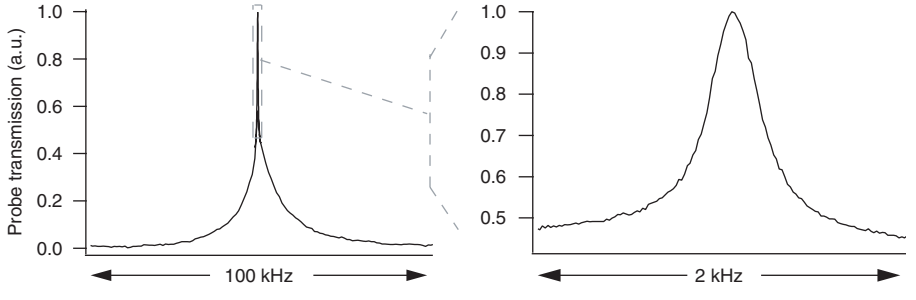

Figure 3. Measured dual-structured EIT lineshape characteristic of a coated cell. The full widths are 13 kHz for the broad structure and 350 Hz for the narrow peak. Note that the narrow peak is substantially narrower than the width of ~10 kHz expected from transit time broadening across the 4.5 mm beam. Control field intensity is 3.5 mW/cm^2 and cell temperature is 48°C; hence the narrow EIT peak is subject to moderate power broadening.

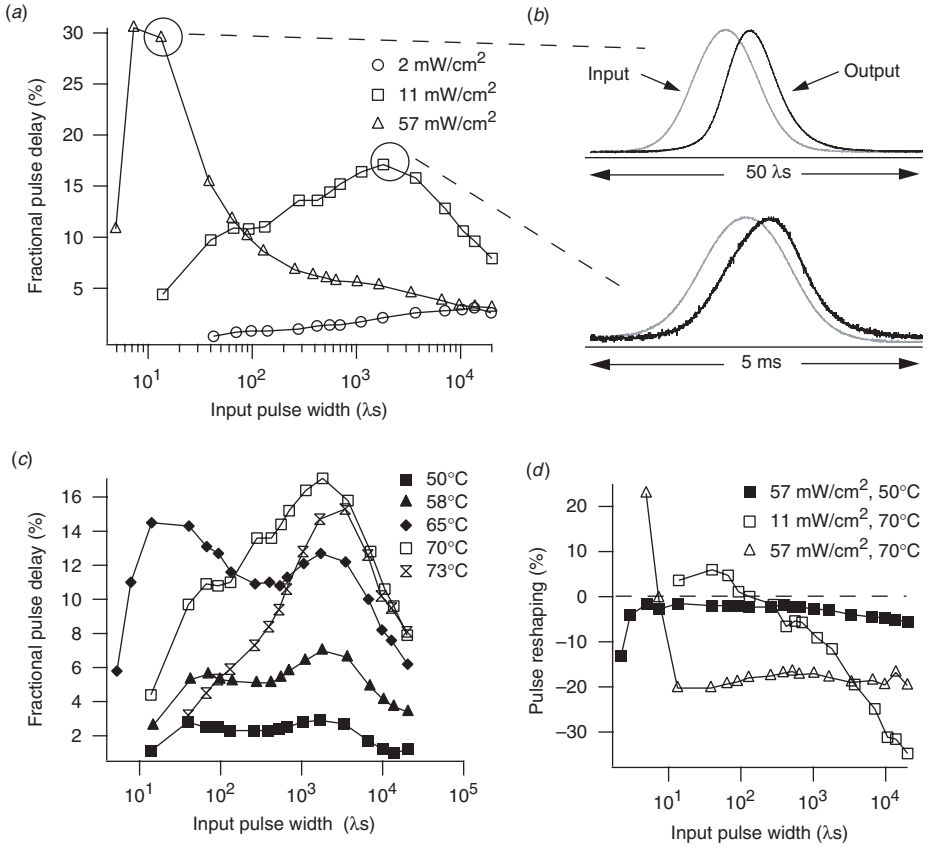

Figure 4. Fractional pulse delay as a function of input pulse width for (*a*) different laser intensities at constant cell temperature (70°C) and (*c*) different cell temperatures at constant laser intensity (11 mW/cm^2). (*b*) Examples of slow light pulse propagation for two maximum fractional delay regimes. (*d*) Slow light pulse reshaping (*see text*). Beam diameter ≈ 2 mm.

using a laser field resonant with the $F = 1 \rightarrow F' = 2$ transition in ^{87}Rb and circularly polarized with the same polarization as the control field. At optimized repumping intensity, the fractional delay of a slow light pulse is increased (figure 5(*b*)); the fractional delay nearly doubles for low densities and therefore relatively low fractional delays (open diamonds in figure 5(*b*)). At higher densities and delays, however, the benefit of the repumping beam is less significant (solid diamonds in figure 5(*b*)).

The maximum fractional pulse delays observed in these coated cells do not exceed 30%. We believe that our observed delays are limited by radiation trapping, i.e. the re-absorption of spontaneous, incoherent photons by the atomic medium [27]. Although fluorescence is suppressed by EIT, spontaneously emitted photons are still present due to residual absorption such as that from other excited state levels [28]. If an atom in the dark state absorbs an unpolarized photon, its coherence is destroyed. Thus radiation trapping effectively increases the ground state decoherence rate,

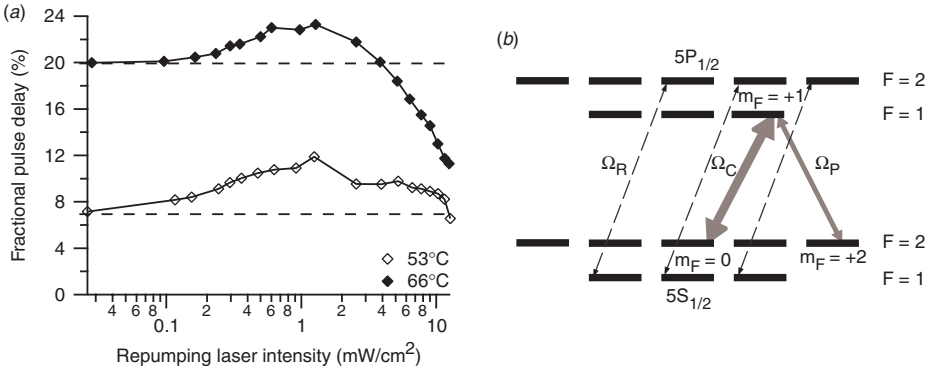

Figure 5. (*a*) ^{87}Rb level scheme showing the repumper (Ω_R) and the fields used in EIT and slow light experiments. (*b*) Slow light fractional delay vs power of repumping laser. Dashed horizontal lines show the fractional delay without repumping laser.

leading to higher absorption, broader EIT linewidth, and shorter pulse delays. Motional averaging of atoms with ground state coherence throughout the vapour cell exacerbates the effects of radiation trapping in coated cells in comparison to buffer gas cells in which atoms participating in the slow light process are typically close to the axis of the cell.

For long pulses (in which the pulse bandwidth is much narrower than the width of the narrow, central EIT feature) we expect the group velocity to be proportional to the control field intensity and inversely proportional to the atomic density [15, 16]. At low atomic densities for which most spontaneous photons are not reabsorbed (squares in figure 6(*a*)) we observe such linear scaling of the group velocity with laser intensity. Similarly, at relatively high laser intensities, for which the additional decoherence due to radiation trapping is insignificant compared to the power-broadened EIT bandwidth, the measured group velocity scales inversely with atomic density (figure 6(*a*)). However, at low control field intensities and high densities the group velocity begins to increase (figure 6(*a*)) as the absorption of the probe beam by the slow light medium becomes substantial (figure 6(*b*)). This observation also explains why improved state selection from the repumping laser has only a limited effect at higher temperature: an increase in the density of appropriately state-selected atoms further enhances absorption of the probe field.

5. Conclusions

We have studied EIT and slow light pulse propagation in paraffin-coated Rb vapour cells, and outlined the methods used in their manufacturing and testing. The long lifetimes for ground-state spin coherence due to the wall coating lead to a narrow central peak in the EIT lineshape and hence ultra-slow group velocity pulse propagation, which in principle should enable very long light delay and storage times.

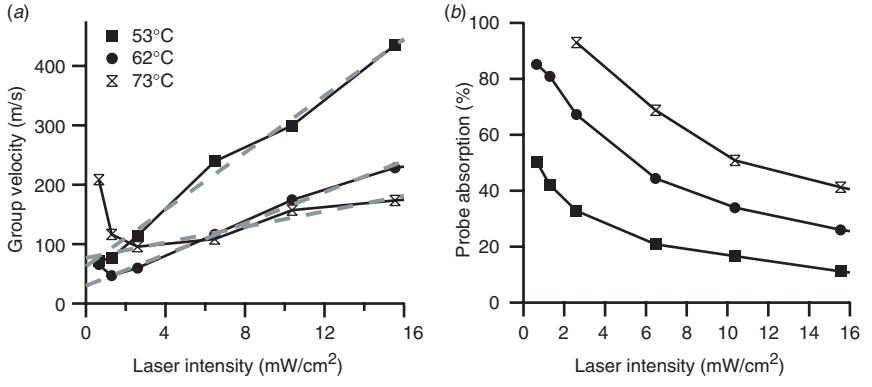

Figure 6. Dependence of (*a*) group velocity and (*b*) pulse absorption on control field intensity for different cell temperatures. Dashed lines indicate linear trending with control field intensity expected without radiation trapping.

To properly describe pulse propagation in a coated cell, both atoms interacting multiple times with the beam after repeated wall collisions and atoms interacting only once with the laser beam must be included. These two interaction timescales correspond to a dual-structured EIT lineshape with two regimes for fractional pulse delay optimization. In our studies to date we believe that radiation trapping is the leading factor limiting observed slow-light fractional delays to $\approx 30\%$. To achieve larger fractional delays in coated cells, we are presently pursuing long, narrow cell geometries and the use of isotopically enriched ^{87}Rb to reduce the role of radiation trapping.

Acknowledgments

The authors are grateful to M. A. Hohensee and Y. Xiao for useful discussions. This work was supported by DARPA, ONR and the Smithsonian Institution.

References

[1] M. O. Scully, and M. S. Zubairy, *Quantum Optics* (Cambridge University Press, Cambridge, 1997).
[2] M. D. Lukin, Rev. Mod. Phys. **75** 457 (2003).
[3] M. A. Bouchiat and J. Brossel, Phys. Rev. **147** 41 (1966).
[4] H. G. Robinson and C. E. Johnson, Appl. Phys. Lett. **40** 771 (1982).
[5] D. Budker, V. Yashchuk and M. Zolotorev, Phys. Rev. Lett. **81** 5788 (1998); D. Budker, L. Hollberg, D. F. Kimball, J. Kitching, S. Pustelny, and V. V. Yashchuk, Phys. Rev. A **71** 012903 (2005); M. T. Graf, D. F. Kimball, S. M. Rochester, K. Kerner, C. Wong, D. Budker, E. B. Alexandrov, M.V. Balabas, and V. V. Yashchuk, Phys. Rev. A **72** 023401 (2005).

[6] A. Kuzmich, L. Mandel, and N. P. Bigelow, Phys. Rev. Lett. **85** 1594 (2000).
[7] B. Julsgaard, A. Kozhekin, and E. S. Polzik, Nature **413** 400 (2001).
[8] C. Schori, B. Julsgaard, J. L. Sorensen *et al*. Phys. Rev. Lett. **89** 057903 (2002).
[9] B. Julsgaard, J. Sherson, J. I. Cirac *et al*. Nature **432** 482 (2004).
[10] H. G. Robinson and C. E. Johnson, IEEE Trans. Instr. Meas. **32** 198 (1983).
[11] E. B. Alexandrov, and V. A. Bonch-Bruevich, Opt. Eng. **31** 711 (1992); E. B. Alexandrov, M. V. Balabas, A. S. Pasgalev, A. K. Vershovskii and N. N. Yakobson, Laser Phys. **6** 244 (1996).
[12] D. Budker, D. F. Kimball, S. M. Rochester *et al*. Phys. Rev. A **62** 043403 (2000).
[13] S. E. Harris, Phys. Today **50**(7) 36 (1997).
[14] J. P. Marangos, J. Mod. Opt. **45** 471 (1998).
[15] A. B. Matsko, O. Kocharovskaya, Y. Rostovtsev *et al*. Adv. Atom. Mol. Opt. Phys. **46** 191 (2001).
[16] R. W. Boyd and D. J. Gauthier, Progress Opt. **43** 497 (2002).
[17] M. Fleischhauer and M. D. Lukin, Phys. Rev. A **65** 022314 (2002).
[18] L.-M. Duan, M. D. Lukin, J. I. Cirac *et al*. Nature **414** 413 (2001).
[19] D. Budker, D. F. Kimball, S. M. Rochester *et al*. Phys. Rev. Lett. **83** 1767 (1999).
[20] H. G. Robinson, E. S. Ensberg and H. G. Dehmelt, Bull. Am. Phys. Soc. **3** 9 (1958).
[21] H. M. Goldenberg, D. Kleppner and N. F. Ramsey, Phys. Rev. **123** 530 (1961).
[22] G. Singh, P. Dilavore and C. O. Alley, Rev. Sc. Instrum. **43** 1388 (1972).
[23] D. F. Phillips, A. Boca and R. L. Walsworth, http://cfa-www.harvard.edu/ dphil/work/ coat.pdf
[24] New Focus Vortex laser model 6017.
[25] W. Demtröder, *Laser Spectroscopy* (Springer, Berlin, 1996).
[26] R. W. Boyd, D. J. Gauthier, A. L. Gaeta *et al*. Phys. Rev. A **71** 023801 (2005).
[27] A. F. Molisch and B. P. Oehry, *Radiation Trapping in Atomic Vapors* (Oxford University Press, New York, 1999); A. B. Matsko, I. Novikova, M. O. Scully and and G. R. Welch, Phys. Rev. Lett. **87** 133601 (2001); A. B. Matsko, I. Novikova and and G. R. Welch, J. Mod. Opt. **49** 367 (2002).
[28] A. B. Matsko, D. V. Strekalov and L. Maleki, Opt. Exp. **13** 2210 (2005).